RESEARCH



Nonlocal Operator Learning for Homogenized Models: From High-fidelity Simulations to Constitutive Laws

Huaiqian You¹ · Yue Yu¹ · Stewart Silling² · Marta D'Elia^{3,4}

Received: 28 August 2023 / Accepted: 21 February 2024
© The Author(s), under exclusive licence to Springer Nature Switzerland AG 2024

Abstract

We show that machine learning can improve the efficacy of simulations of stress waves in one-dimensional composite materials. We propose a data-driven technique to learn nonlocal constitutive laws, which act as a homogenized surrogate for stress wave propagation models. The method is an optimization-based technique in which the nonlocal kernel function is approximated via Bernstein polynomials. The kernel, including both its functional form and parameters, is derived so that when used in a nonlocal solver, it generates solutions that closely match high-fidelity data. The optimal kernel therefore acts as a homogenized nonlocal continuum model that accurately reproduces wave motion in a smaller-scale, more detailed model that can include multiple materials. We apply this technique to wave propagation within a heterogeneous bar with a periodic microstructure. Several one-dimensional numerical tests illustrate the accuracy of our algorithm. The optimal kernel is demonstrated to reproduce high-fidelity data for a composite material in applications that are substantially different from the problems used as training data.

Keywords Wave propagation \cdot Data-driven learning \cdot Nonlocal operator regression \cdot Homogenization \cdot Nonlocal models

1 Introduction

Nonlocal models use integral operators acting on a lengthscale δ , known as horizon. This feature allows nonlocal models to capture long-range forces at small scales and multiscale behavior, and to reduce regularity requirements on the solutions, which are allowed to be discontinuous or even singular. In recent decades, nonlocal equations have been successfully used to model several engineering and scientific applications, including fracture mechanics [1–3], subsurface transport [4, 5], image processing [6, 7], multiscale and multiphysics systems [8–10], finance [11], and stochastic processes [12, 13].

However, it is often the case that *nonlocal kernels* defining nonlocal operators are justified a posteriori and it is not clear how to define such kernels to faithfully describe a physical system. The problem of learning an appropriate kernel for a specific application is one of

✓ Yue Yu yuy214@lehigh.edu

Extended author information available on the last page of the article

Published online: 10 April 2024



the most challenging open problems in nonlocal modeling. The literature on techniques for learning kernel *parameters* for a given functional form is vast, see, e.g., [14, 15] for control-based approaches, and [16, 17] for machine-learning approaches. However, the use of machine learning to learn the *functional form* of the kernel is still in its infancy, [18–20] being the only relevant works that we are aware of.

In this work we use an approach similar to the one developed in [20] to learn nonlocal kernels whose associated nonlocal wave equation is well posed by construction and can be used as an accurate surrogate for more detailed, high-fidelity wave propagation models. In particular, we present an application to wave propagation at the microscale in a heterogeneous solid. In this context, the machine-learned nonlocal kernel embeds the material constitutive behavior so that the material interfaces do not have to be treated explicitly and, more importantly, the material microstructure can be unknown. Furthermore, the corresponding nonlocal models allow for accurate simulations at scales that are much larger than the microstructure.

Our main contributions are:

- The design of an optimization technique that bridges micro and continuum scales by providing accurate and stable homogenized surrogate models for the simulation of wave propagation in heterogeneous materials.
- The illustration of this method via one-dimensional experiments that confirm the applicability of our technique and the improved accuracy compared with state-of-the-art results.
- The demonstration of generalization properties of our algorithm whose associated model surrogates are effective even on problem settings that are substantially different from the ones used for training in terms of loading and time scales.

2 Nonlocal Kernel Learning

We introduce the high-fidelity (HF) model that faithfully represents the system: for $\Omega \in \mathbb{R}^d$, the scalar function u(x,t) solves, for $(x,t) \in \Omega \times [0,T]$

$$\frac{\partial^2 u}{\partial t^2}(x,t) - \mathcal{L}_{HF}[u](x,t) = f(x,t), \tag{1}$$

provided some boundary conditions on $\partial\Omega$ for u(x,t) and initial conditions at t=0 for u and $\partial u/\partial t$ are satisfied. Here, \mathcal{L}_{HF} is the HF operator, which can either be a differential or integral operator, and f represents a forcing term.

We assume that solutions to this HF problem may be approximated by solutions to a nonlocal problem of the form

$$\frac{\partial^2 u}{\partial t^2}(x,t) - \mathcal{L}_K[u](x,t) = f(x,t),\tag{2}$$

for $(x, t) \in \Omega \times [0, T]$, augmented with nonlocal boundary conditions on Ω_{δ} (a layer of thickness δ that surrounds the domain) and the same initial conditions on the variable u and its derivative as in (1). The forcing f may coincide with the forcing term in (1) or it could be an appropriate representation of the same.

We seek \mathcal{L}_K as a nonlocal operator of the form

$$\mathcal{L}_K[u](x,t) = \int_{\overline{\Omega}} K(|x-y|) \left(u(y,t) - u(x,t) \right) \, dy \tag{3}$$

where K is a radial, sign-changing, *kernel function*, compactly supported on the ball of radius δ centered at x, i.e., $B_{\delta}(x)$ and $\overline{\Omega} = \Omega \cup \Omega_{\delta}$.



2.1 The Algorithm

To learn the kernel K, we assume that we are given N pairs of forcing terms and corresponding solutions to (1), normalized with respect to the L^2 norm of each solution over $\Omega \times [0, T_{\rm tr}]$. These are denoted by

$$\mathcal{D}_{tr} = \{ (u_k(x, t), f_k(x, t)) \}_{k=1}^N,$$
(4)

for $x \in \Omega$ and $t \in (0, T_{tr}]$. Similarly to [20], we represent K as a linear combination of Bernstein basis polynomials:

$$K\left(\frac{|y|}{\delta}\right) = \sum_{m=0}^{M} \frac{C_m}{\delta^{d+2}} B_{m,M}\left(\left|\frac{y}{\delta}\right|\right),\tag{5}$$

where the Bernstein basis functions are defined as

$$B_{m,M}(x) = {M \choose m} x^m (1-x)^{M-m} \text{ for } 0 \le x \le 1$$

and where $C_m \in \mathbb{R}$. Note that, by construction, this kernel guarantees that (2) is well-posed [21].

We machine-learn the nonlocal model by finding optimal parameters $\{C_m\}$ such that solutions \hat{u}_k to (2), for $f = f_k$ and the kernel function K associated to $\{C_m\}$, are as close as possible to the training variable u_k .

In this work we numerically approximate \hat{u}_k by \bar{u}_k using a central-differencing scheme in time with time step dt, i.e.

$$\bar{u}_k^{n+1}(x_i) = 2\bar{u}_k^n(x_i) - \bar{u}_k^{n-1}(x_i) + dt^2 \left(\mathcal{L}_{K,h}[\bar{u}_k^n](x_i) + f_k(x_i, t^n) \right), \tag{6}$$

where $\bar{u}_k^{n+1}(x_i)$ represents the k-th approximate solution at time step t^{n+1} and at discretization point x_i , and $\mathcal{L}_{K,h}$ is an approximation of \mathcal{L}_K by Riemann sum with uniform grid spacing h. The optimal parameters are obtained by solving the following optimization problem.

$$\min_{C_m} \frac{T_{\text{tr}}}{dt^3 N} \sum_{k=1}^{N} \sum_{n=1}^{T_{\text{tr}}/dt} \left\| \bar{u}_k^{n+1} - u_k(t^{n+1}) \right\|_{\ell^2}^2 + \mathcal{R}(\{C_m\}), \tag{7}$$

s.t.
$$\bar{u}_k$$
 satisfies (6) and (8)

Here, the ℓ^2 norm is taken over the space-discretization points x_i , and (9) depends on the physics of the problem (as an example, it may correspond to enforcing that the surrogate model reproduces exactly a certain class of solutions). $\mathcal{R}(\cdot)$ is a regularization term on the coefficients that improves the conditioning of the optimization problem. In this paper, we adopt the classical practice in machine learning and employ the Tikhonov regularizer using the ℓ^2 norm of trainable parameters: $\mathcal{R}(\{C_m\}) := \frac{\epsilon}{M+1} \sum_{m=0}^M C_m^2$, where the regularization weight ϵ is chosen empirically to guarantee accurate predictions, as we explain later on. We also point out that when additional knowledges, such as the prior knowledge about kernel [22] or the information from data [23], are available, more advanced regularization terms can be proposed accordingly.



3 Dispersion in Heterogeneous Materials

We apply the learning algorithm described above to the propagation of waves in a onedimensional heterogeneous bar, like the one reported in Fig. 1, with an *ordered* microstructure, i.e. two materials with the same length alternate periodically. Our goal is to learn a nonlocal model able to reproduce wave propagation on distances that are much larger than the size of the microstructure without resolving the microscales. The high-fidelity model we rely on is the classical wave equation; the corresponding high-fidelity data used for training and validation are obtained with the solver described below.

3.1 High-fidelity Data

For both training and validation purposes we generate data using high-fidelity simulations for the propagation of stress waves within the microstructure of the heterogeneous, linear elastic bar. This method, which will be referred to as Direct Numerical Solution (DNS), constructs an arbitrarily complex wave diagram (also called an x-t diagram), that treats the mutual interaction and superposition of many wavefronts moving in either direction. The bar is discretized into nodes such that it takes a constant amount of time Δt for a wave to travel between nodes γ and $\gamma + 1$, regardless of the elastic wave speed in the material between these two nodes. Therefore, in a heterogeneous medium, the spacing between nodes is not constant. Each node γ , at each time step n, has velocity v_{ν}^{n} (note that, in this case, the subscript refers to position, as opposed to the previous section where it corresponds to a specific sample k). To compute the velocities in the next time step, it is assumed that two waves moving in opposite directions converge on the node γ at time step n (see Fig. 2). The waves shown in the figure can have unequal slopes on the x-t diagram because the materials on either side of node γ can have different waves speeds c. The jump conditions for the waves are applied that relate the stress change $[\sigma]$ across a wave to the velocity change [v]. These jump conditions have the following form:

$$[\sigma] = \pm \rho c[v].$$

where ρ is the mass density, and where the + and - signs apply to right-running waves and left-running waves respectively. From these conditions, the velocity v_{γ}^{n+1} can be computed explicitly from the values at the adjacent nodes in time step n-1. Externally applied forces can also be included in a straightforward way. After v_{γ}^{n+1} is computed, the updated displacement is approximated by

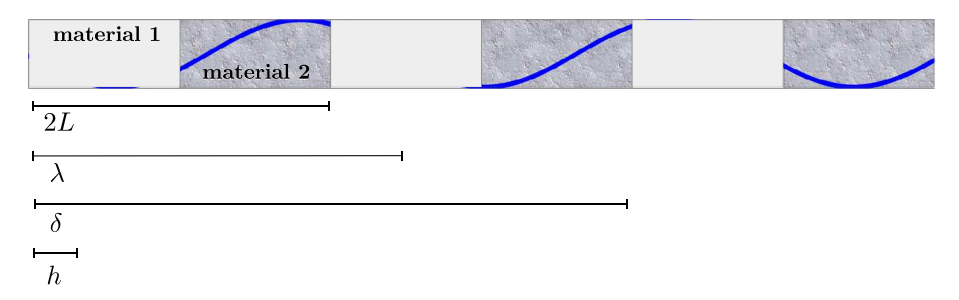
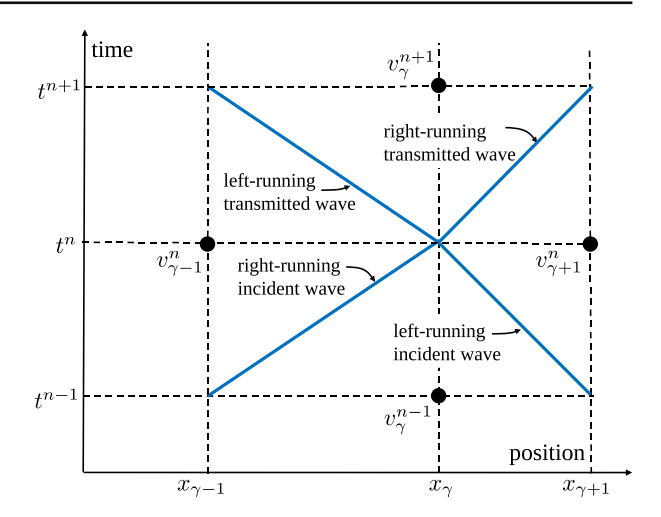


Fig. 1 One-dimensional bar with ordered microstructure of period 2L. Material 1 and 2 have the same density and Young modulus E_1 and E_2 . The horizon δ , the wave length λ , and the discretization size, h, are reported for comparison



Fig. 2 Interaction of two waves in the DNS method. Each node may or may not be located at a material interface



$$u_{\gamma}^{n+1} = u_{\gamma}^n + \Delta t v_{\gamma}^{n+1}.$$

Details of the method can be found in [24].

This DNS solver has the important advantage of not using an approximate representation of derivatives in space or time for the computation of the velocity, which is, therefore, free from truncation error and other sources of discretization error that are usually encountered with PDE solvers. This allows us to model the propagation of waves through many thousands of microstructural interfaces without the need to worry about what features of the velocity are real and what are numerical artifacts.

We consider four types of data and use the first two for training and the last two for validation of our algorithm. In all our experiments we set L=0.2, $E_1=1$, $E_2=0.25$, $\rho=1$, and the symmetric domain $\Omega=(-b,b)$. Discretization parameters for the DNS solver are set to $\Delta t=0.01$ and $\max{\{\Delta x\}}=0.01$.

1. Oscillating source. We set b = 50, v(x, 0) = u(x, 0) = 0,

$$f(x,t) = e^{-\left(\frac{2x}{5kL}\right)^2} e^{-\left(\frac{t-t_0}{t_p}\right)^2} \cos^2\left(\frac{2\pi x}{kL}\right), \ k = 1, 2, \dots, 20, \ t_0 = t_p = 0.8.$$

- 2. *Plane wave.* For b = 50, f(x, t) = 0 and u(x, 0) = 0, we prescribe $v(-b, t) = \sin(\omega t)$ for $\omega = 0.35, 0.7, \dots, 3.85$.
- 3. Wave packet. For b = 133.3, f(x, t) = 0 and u(x, 0) = 0, we prescribe $v(-b, t) = \sin(\omega t) \exp(-(t/5 3)^2)$ for $\omega = 2, 3.9, 5$.
- 4. *Impact*. For b = 266.6, f(x, t) = 0 and u(x, 0) = 0, we prescribe v(x, 0) = 1 for all $x \in [-b, -b + 1.6]$ and v = 0 outside of this interval. This initial condition represents an impactor hitting the bar at time zero, generating a velocity pulse of width roughly 3.2 that propagates into the interior of the bar. The pulse attenuates and changes shape as it encounters the many microstructural interfaces.

3.2 Training Procedure

For the optimization problem (7) we choose a Tikhonov regularization of the form $\mathcal{R}(\{C_m\})$ = $\frac{\epsilon}{M+1}\sum_{m=0}^{M}C_m^2$. The physics-based constraints in (9) are defined as follows and also



discretized by Riemann sum; they are used to explicitly prescribe values of C_{M-1} and C_M :

$$\sum_{m=0}^{M} C_m \int_0^{\delta} \frac{y^2}{\delta^3} B_{m,M} \left(\frac{|y|}{\delta}\right) dy = \rho c_0^2,$$

$$\sum_{m=0}^{M} C_m \int_0^{\delta} \frac{y^4}{\delta^3} B_{m,M} \left(\frac{|y|}{\delta}\right) dy = -4\rho c_0^3 R,$$
(10)

where ρ is the density and c_0 is the effective wave speed for infinitely long wavelengths. For $\rho=1$, it is given by $c_0=(2/(1/E_1+1/E_2)^{\frac{1}{2}}.R$ is the second derivative of the wave group velocity with respect to the frequency ω evaluated at $\omega=0$. Both parameters are obtained by simulating a very low frequency plane wave propagating through the microstructure over a long distance using DNS [24]. These parameters primarily affect simulations at large times, t>10. However, due to practical limitations on computer resources, our training simulations are restricted to $t\leq 2$. Therefore, we incorporate these parameters as constraints obtained from DNS as indicated in (10), rather than attempting to learn these through our algorithm. The first constraint in (10) is also used for similar purposes in [19] and prescribed in a weak sense by penalization.

Training is performed with DNS data of type 1) and 2). Parameters for the nonlocal solver and the optimization algorithm are set to h = 0.05, dt = 0.02, $T_{tr} = 2$, $\delta = 1.2$, M = 24 and $\epsilon = 0.01$. The optimization problem (7) is solved with L-BFGS. Note that we empirically choose δ and ϵ in such a way that the group velocity, defined below, corresponding to the optimal kernel is as close as possible to the one computed with DNS.

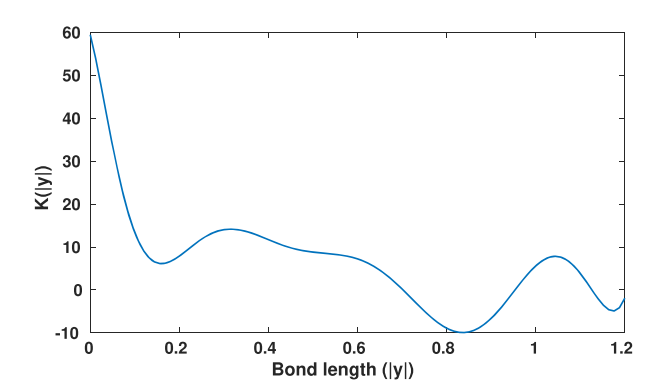
The optimal kernel, $K_{\rm opt}$, is reported in Fig. 3; as expected from the literature [18–20, 25], we observe a sign-changing behavior. We also compute the corresponding dispersion $\omega(k)$ and group velocity $v_g(\omega) = d\omega/dk$. For a given kernel K and different frequencies $k_i = 0$, $\frac{2\pi}{200h}, \cdots, \frac{2\pi}{h}$, the corresponding angular frequency $\omega(k_i)$ and group velocity $v_g(\omega(k_i))$ are approximated by

$$\omega(k_i)^2 \approx \frac{1}{\rho} \sum_q K(|y_q|) (1 - \cos(k_i y_q)) h,$$

$$v_g(\omega(k_i)) \approx \frac{\omega(k_{i+1}) - \omega(k_{i-1})}{k_{i+1} - k_{i-1}},$$

where y_q belong to a uniform grid of size h in $(-\delta, \delta)$.

Fig. 3 Optimal kernel K_{opt} as a function of distance





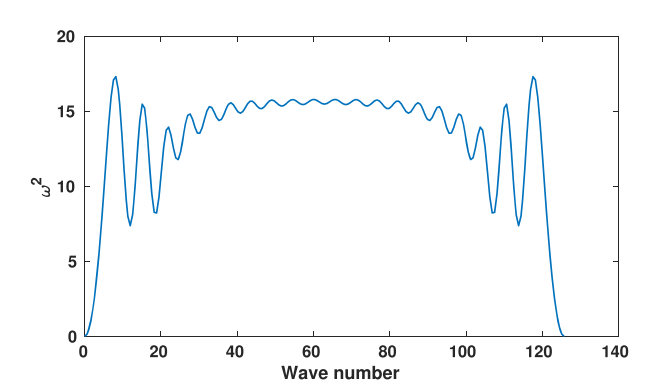
The dispersion curve is reported in Fig. 4, its positivity indicates that $K_{\rm opt}$ corresponds to a physically stable material model. The group velocity is reported in the upper plot of Fig. 5 in comparison with the curve computed with DNS by observing the speed of a wave packet of a given frequency as it moves through the microstructure. We also display the group velocities associated with two alternative kernels obtained for the same material by a completely different method [24]. The first alternative kernel is a constant, specifically, we have that $C_m = K_{\rm const} = 0.7714$ for $\delta = 0.15$. For the second alternative kernel we consider a singular kernel which has been widely studied in nonlocal models (see, e.g., [3, 26]): $K_{\rm singular}(y) = \frac{C}{\delta^2 |y|}$, for C = 0.6 and $\delta = 0.15$.

It is well known that layered, periodic elastic media have a band structure for wave propagation, see [27, pages 121–122]. In the present study, because it is not possible to reproduce the higher-frequency pass bands with the coarse discretization that is used in fitting our nonlocal kernel, we address only the first, low-frequency pass band, i.e. $\omega \in (0, \omega_{bs})$, where "bs" stands for band stop. Hence, the optimal kernel is suitable only for wavelengths that are bigger than the microstructure; this is enough to reproduce the physically most important features of wave propagation in layered media for typical applications.

The profile of the group velocity shows the improved accuracy of our optimal kernel that not only matches the behavior for low values of ω , but also catches the behavior at $\omega = \omega_{\rm bs} \approx 4$. This fact has important consequences on the ability to reproduce wave propagation for values of ω bigger than $\omega_{\rm bs}$. In order to justify the statement above on the optimality of the parameters δ and ϵ , we report the group velocity profile in correspondence of different pairs; it is clear from the profiles in Fig. 5 that $(\delta, \epsilon) = (1.2, 0.01)$ provides the best match both in terms of curvature at $\omega = 0$ and identification of the band stop. One can also see the when the regularization weight, ϵ , is too strong, it leads to a under-fitting to the DNS data: there is a large discrepancy between the group velocities of the learnt kernel and the DNS data. On the other hand, a too-small ϵ would lead to over-fitting. In this case, the model gives accurate predictions for training data by memorizing the noise, and hence the model would not perform well for new data. Such an undesired performance can be probed from the group velocity. As demonstrated by the group velocity of the $(\delta, \epsilon) = (1.2, 0.0001)$ case: the group velocity almost overlaps with the ground truth, but the band stop does not match well. In the following simulations, we will take the result from $(\delta, \epsilon) = (1.2, 0.01)$ as the optimal kernel, $K_{\rm opt}$.

To further demonstrate the training procedure, in Fig. 6 we report the convergence properties of the learning algorithm by showing the history training loss in (7). One can see that the L-BFGS algorithm reaches a plateau within 5 epochs. We also conduct a sensitivity analysis

Fig. 4 Dispersion curve associated with K_{opt}





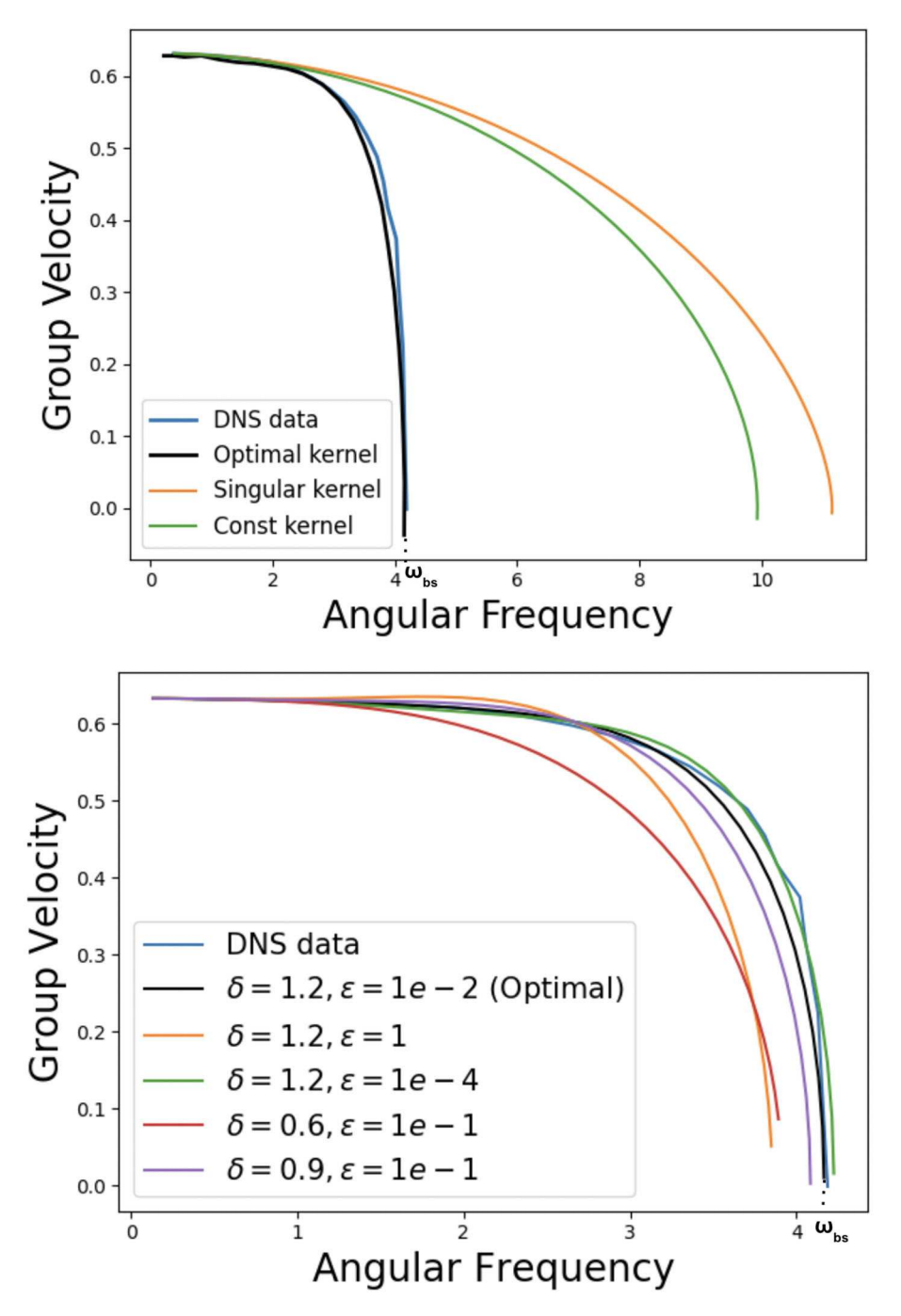
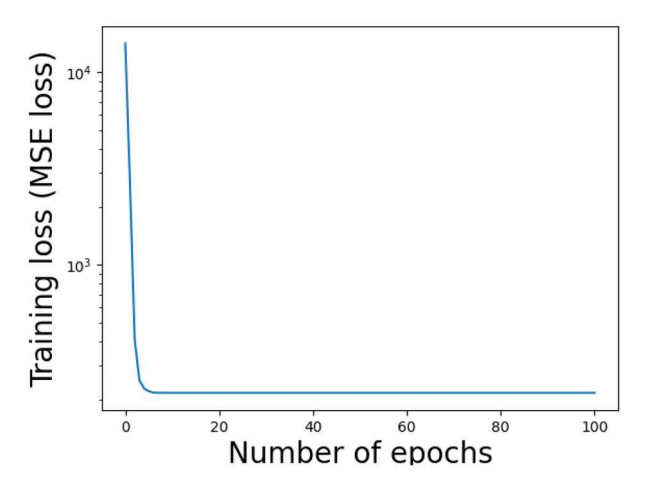


Fig. 5 Comparison of the group velocity. Upper: group velocity corresponding to $K_{\rm opt}$, $K_{\rm const}$, $K_{\rm singular}$, and DNS data. Bottom: group velocity corresponding to $K_{\rm opt}$ for different pairs (δ,ϵ)



Fig. 6 Optimization history of K_{opt} , using the L-BFGS algorithm and the training loss following (7)

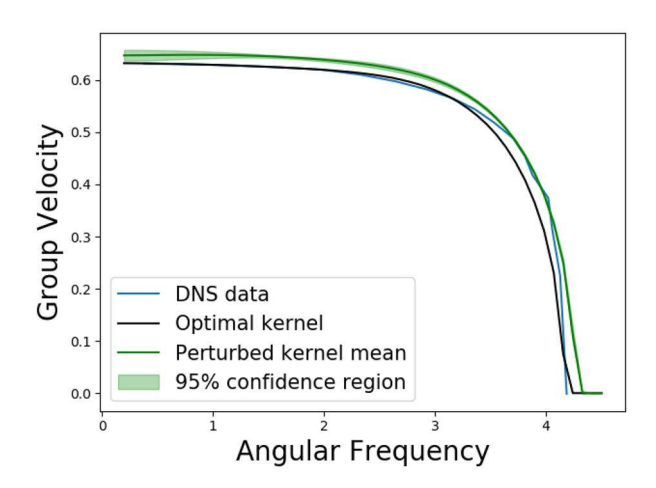


for the optimal kernel parameter set $\{C_m\}_{m=0}^M$, and demonstrate the results in Fig. 7. Here, we add an additive noise to the optimal kernel parameter set as $\{C_m(1+\epsilon)\}$, where ϵ is a random variable satisfying the uniform distribution: $\epsilon \sim \mathcal{U}[-0.1, 0.1]$. We generate 100 realizations of perturbed kernels, then report their averaged group velocity and 95% confidence region. Because the perturbation introduces errors on the two physical constraints (10), the resultant group velocity does not guarantee a perfect match with the DNS data at the low frequency end, as can be seen from the averaged group velocity curve in Fig. 7. On the other hand, the confidence region almost coincides with the averaged group velocity. This fact demonstrates that the wave dispersion behavior has a low sensitivity to the perturbation of kernel parameters.

3.3 Numerical Validation

We test the performance of the optimal kernel $K_{\rm opt}$ on data sets of type 3) and 4), i.e. the problem setting considered for validation has different model parameters, including the domain, than the one used for training and, hence, these tests serve as an indicator of the generalization properties of our algorithm.

Fig. 7 Sensitivity analysis of K_{opt} , where we perturb the optimal kernel parameter set $\{C_m\}_{m=0}^M$ by 10%, then calculate the averaged group velocity and 95% confidence region from 100 realizations





Wave packet For data type 3) we numerically compute solutions to (2) using $K_{\rm opt}$ and DNS data as nonlocal boundary conditions. We consider solutions corresponding to three values of ω : $\omega_1 = 2 < \omega_{\rm bs}$, $\omega_2 = 3.9 \approx \omega_{\rm bs}$ and $\omega_3 = 5 > \omega_{\rm bs}$. Note that the latter value is beyond the band stop and, as such, corresponds to a zero group velocity, i.e. the wave does not travel in time. In Fig. 8 we report the velocity corresponding to the computed displacement \bar{u} at time t = 100, t = 320, and t = 100 for ω_1 , ω_2 , and ω_3 respectively; as a reference, we also report the exact DNS velocity. Our results indicate that our kernel can accurately reproduce solutions of type 3) at times larger than $T_{\rm tr}$ and for all values of ω , even larger than $\omega_{\rm bs}$. This is possible because the group velocity corresponding to $K_{\rm opt}$ reproduces the true group velocity very accurately, see Fig. 5. In particular, detecting the presence of a band stop allows us to accurately predict the wave propagation for values of $\omega > \omega_{\rm bs}$. Due to the poor accuracy of the group velocity associated to the two baseline kernels, $K_{\rm const}$ and $K_{\rm singular}$, corresponding

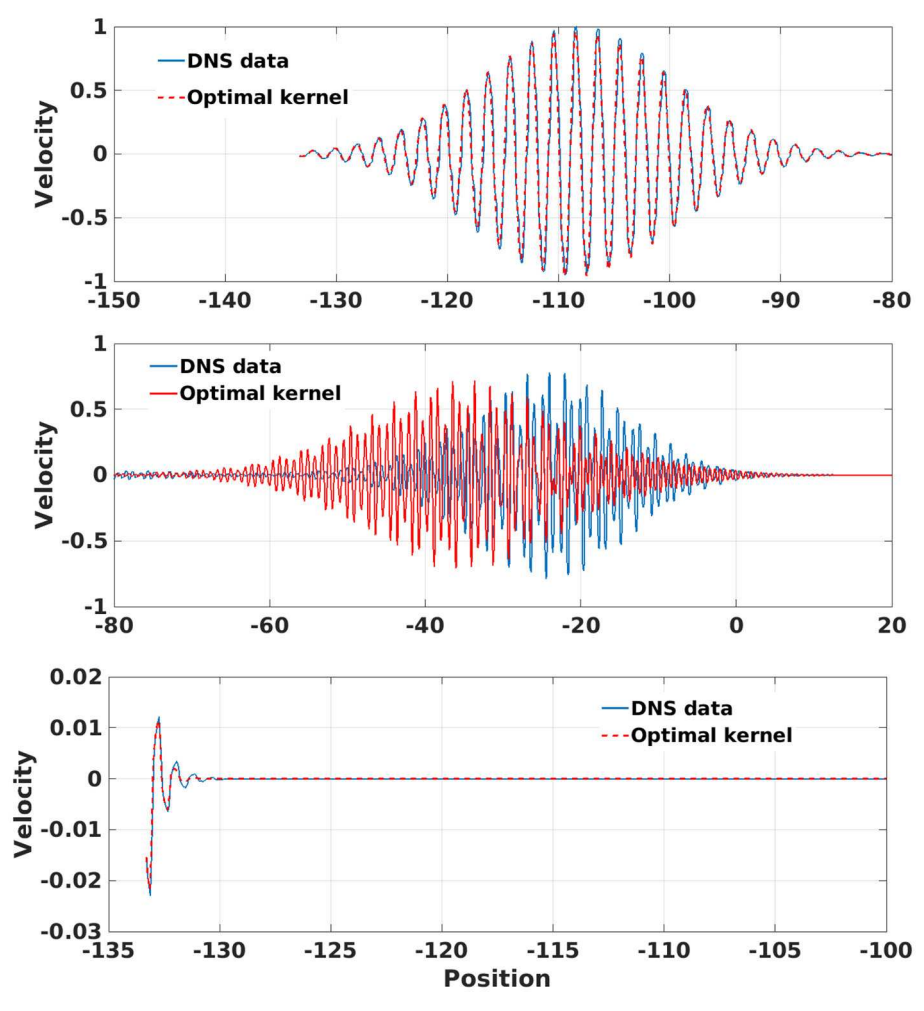


Fig. 8 Velocity computed with K_{opt} . Plots from top to bottom correspond to: 1. $\omega_1 = 2$ at t = 100; 2. $\omega_2 = 3.9$ at t = 320; 3. $\omega_3 = 5$ at t = 100



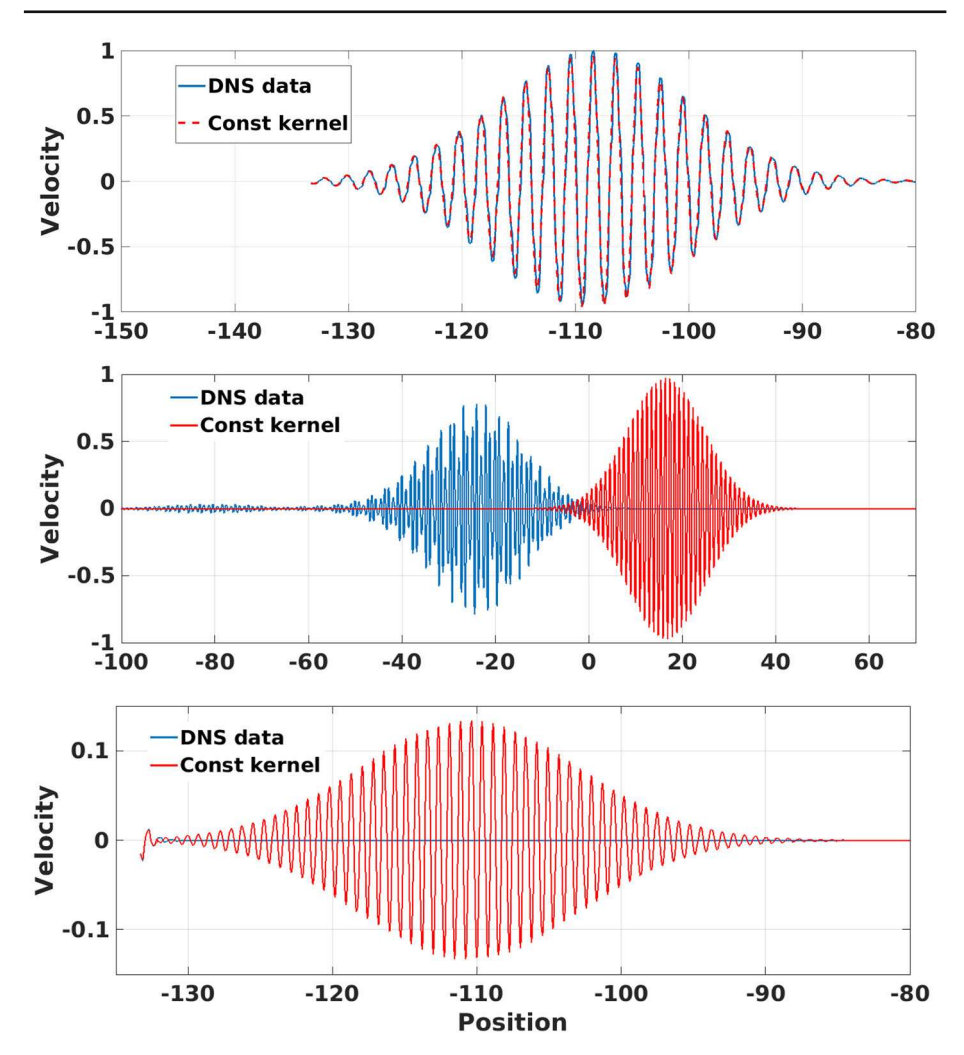


Fig. 9 Velocity computed with K_{const} . Plots from top to bottom correspond to: 1. $\omega_1 = 2$ at t = 100; 2. $\omega_2 = 3.9$ at t = 320; 3. $\omega_3 = 5$ at t = 100. The optimal kernel K_{opt} obtained by machine learning (Fig. 8) clearly performs better than K_{const} for the second and third cases (ω_2 and ω_3)

solutions are not as accurate for ω in the proximity of $\omega_{\rm bs}$ and beyond. To illustrate this phenomenon, we report in Fig. 9 the behavior of the velocity corresponding to $K_{\rm const}$ at time t=100, t=320 and 100, respectively for ω_1, ω_2 and ω_3 . Comparison with DNS data shows that, for ω_2 the wave associated with $K_{\rm const}$ is traveling faster than the exact one and, for ω_3 , it keeps traveling while the exact wave is not propagating. Similar phenomenon is observed for $K_{\rm singular}$, as shown in Fig. 10.



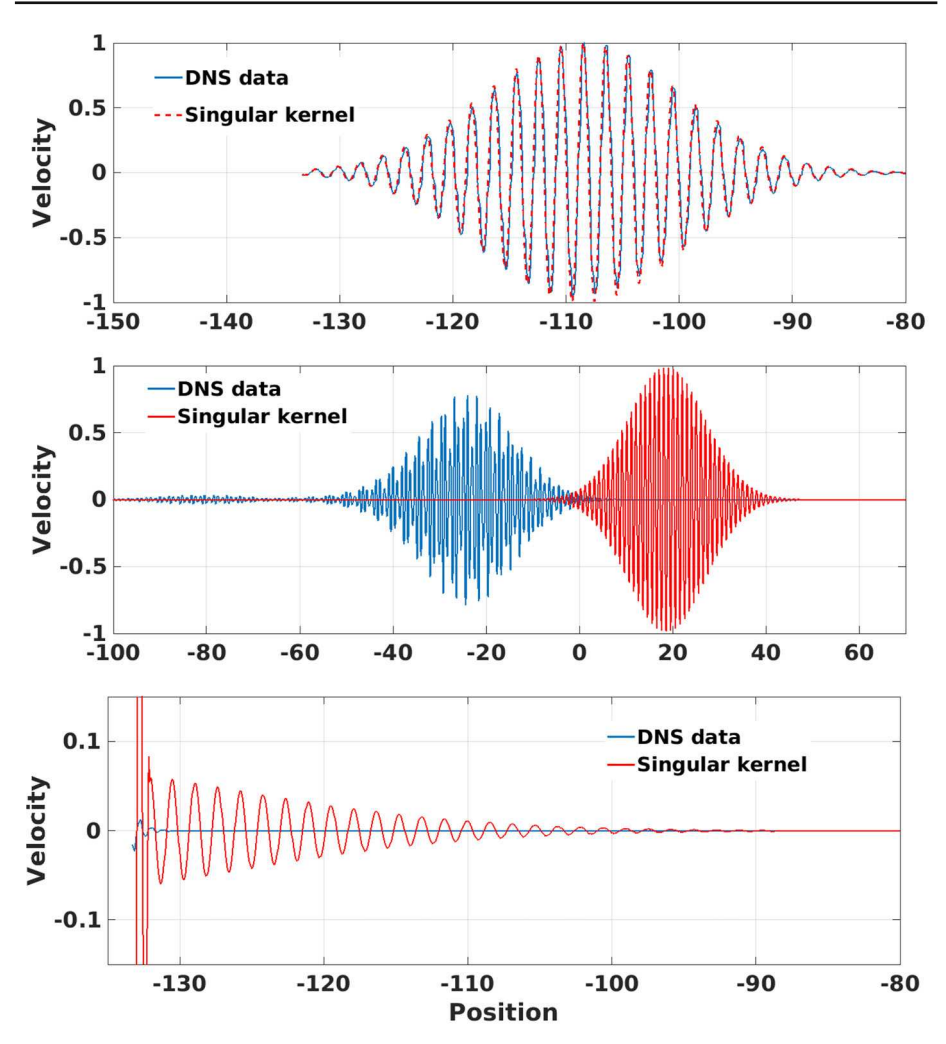


Fig. 10 Velocity computed with K_{singular} . Plots from top to bottom correspond to: 1. $\omega_1 = 2$ at t = 100; 2. $\omega_2 = 3.9$ at t = 320; 3. $\omega_3 = 5$ at t = 100. The optimal kernel K_{opt} obtained by machine learning (Fig. 8) again performs better than K_{singular}

Impact We use the optimal kernel to compute solutions corresponding to data type 4). In Fig. 11 we report the velocity profile at different time steps in correspondence of $K_{\rm opt}$ and DNS data, displayed for comparison. Figs. 12 and 13 display the same results in correspondence of $K_{\rm const}$ and $K_{\rm singular}$, respectively. These results indicate that our optimal kernel can accurately predict the short- and long-time wave propagation, as opposed to the constant kernel that successfully predicts the long-time behavior only, and the singular kernel that overly predicts the size of oscillations that trail the main pulse in both short-time and long-time simulations. We also point out that for values of (δ, ϵ) for which the group velocity is not accurate, the predicted velocity and displacement exhibit non-physical oscillations, which disappear in correspondence of pairs that guarantee an accurate group velocity profile.



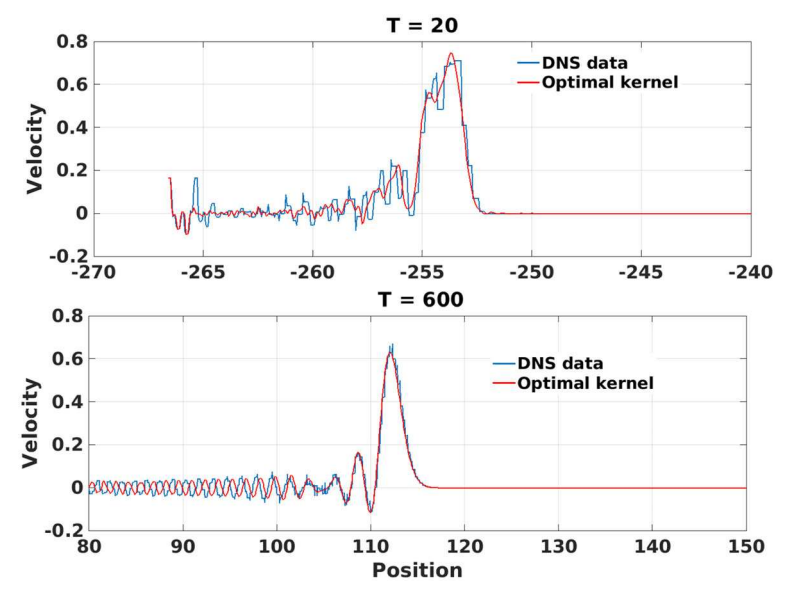


Fig. 11 Velocity profile for the *Impact* problem at T = 20 and T = 600 with K_{opt}

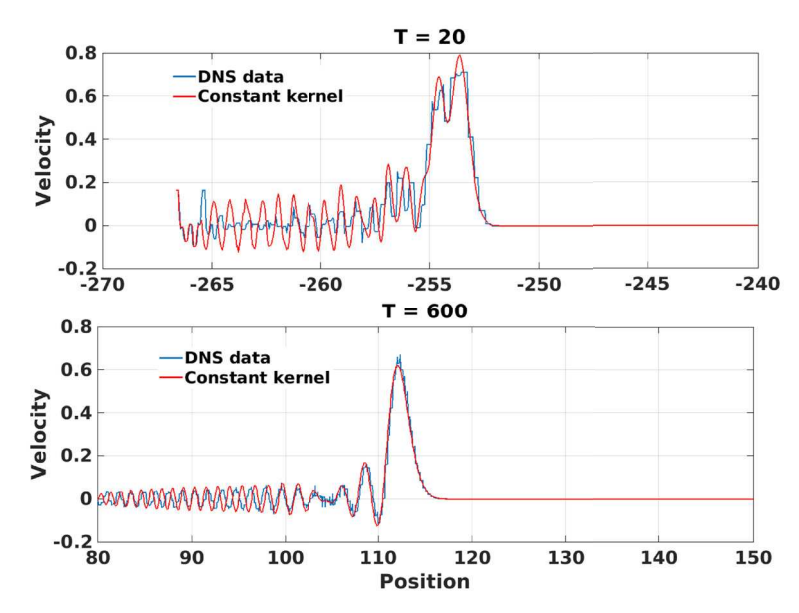


Fig. 12 Velocity profile for the *Impact* problem at T=20 and T=600 with $K_{\rm const}$. The optimal kernel $K_{\rm opt}$ obtained by machine learning (Fig. 11) provides better agreement with the DNS data than $K_{\rm const}$ at the earlier time (T=20) by reducing the size of the oscillations that trail the main pulse. For large T, the solution is dominated by the low frequency components of the pulse, for which the two kernels behave similarly



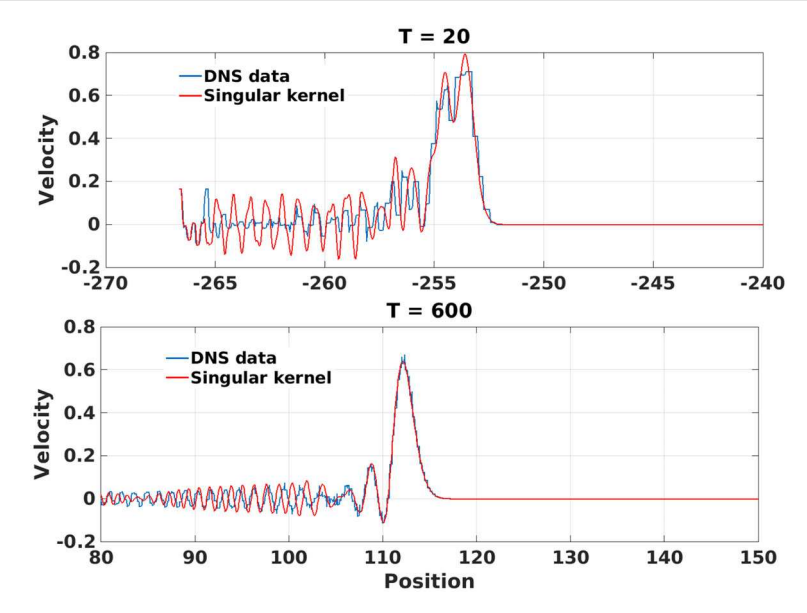


Fig. 13 Velocity profile for the *Impact* problem at T=20 and T=600 with $K_{\rm singular}$. The optimal kernel $K_{\rm opt}$ obtained by machine learning (Fig. 11) provides better agreement with the DNS data than $K_{\rm singular}$ at both the earlier time (T=20) and the later time (T=600), since the later overly predicts the size of oscillations that trail the main pulse

4 Conclusion

We introduced a new data-driven, optimization-based algorithm for the identification of nonlocal kernels in the context of wave propagation through material featuring heterogeneities at the microscale. The corresponding nonlocal model is well-posed by construction and allows for accurate simulations at a larger scale than the microstructure. We stress the fact that our algorithm does not require a priori knowledge of the microstructure (often unknown and/or hard to model), but only requires high-fidelity measurements of the displacements or the velocity. We also point out that our algorithm has excellent generalization properties as the optimal kernel performs well at much larger times than the time instants used for training and on problem settings that are substantially different from the training data set.

One of the most important findings in this work is the key role of the group velocity in the accuracy of the predictions; in fact, our criterion for the choice of the horizon δ and the regularization weight ϵ is the accurate prediction of the group velocity profile. Given the critical role of such quantity, our future work includes the identification of the optimal horizon by, possibly, embedding constraints on the group velocity to the training procedure. Another natural follow-up work is the illustration of the efficiency of our algorithm on two-and three-dimensional test cases.

Author Contributions HY: Software, Methodology, Programming, Analysis. YY: Methodology, Supervision, Conceptualization, Analysis. SS: Dataset, Software, Analysis. MD: Writing, Conceptualization.

Funding HY and YY are supported by the National Science Foundation under award DMS 1753031 and the AFOSR grant FA9550-22-1-0197. Portions of this research were conducted on Lehigh University's Research Computing infrastructure partially supported by NSF Award 2019035. MD and SS are supported by the Sandia National Laboratories (SNL) Laboratory-directed Research and Development program and by the U.S.



Department of Energy, Office of Advanced Scientific Computing Research under the Collaboratory on Mathematics and Physics-Informed Learning Machines for Multiscale and Multiphysics Problems (PhILMs) project. SNL is a multimission laboratory managed and operated by National Technology and Engineering Solutions of Sandia, LLC., a wholly owned subsidiary of Honeywell International, Inc., for the U.S. Department of Energy's National Nuclear Security Administration under contract DE-NA-0003525. This paper, SAND2020-13633, describes objective technical results and analysis. Any subjective views or opinions that might be expressed in this paper do not necessarily represent the views of the U.S. Department of Energy or the United States Government.

Data Availability All datasets and codes will be made available on reasonable request.

Declarations

Ethical Approval Not applicable, since this paper does not involve any human nor animal studies.

Competing Interests The authors declare no competing interests.

References

- Silling SA (2000) Reformulation of elasticity theory for discontinuities and long-range forces. J Mech Phys Solids 48(1):175–209
- Ha YD, Bobaru F (2011) Characteristics of dynamic brittle fracture captured with peridynamics. Eng Fract Mech 78(6):1156–1168
- Trask N, You H, Yu Y, Parks ML (2019) An asymptotically compatible meshfree quadrature rule for nonlocal problems with applications to peridynamics. Comput Methods Appl Mech Eng 343:151–165
- Benson D, Wheatcraft S, Meerschaert M (2000) Application of a fractional advection-dispersion equation. Water Resour Res 36(6):1403–1412
- Schumer R, Benson D, Meerschaert M, Baeumer B (2003) Multiscaling fractional advection-dispersion equations and their solutions. Water Resour Res 39(1):1022–1032
- D'Elia M, De los Reyes JC, Trujillo AM (2019) Bilevel parameter optimization for nonlocal image denoising models. Preprint at http://arxiv.org/abs/1912.02347
- Gilboa G, Osher S (2007) Nonlocal linear image regularization and supervised segmentation. Multiscale Model Simul 6:595–630
- Alali B, Lipton R (2012) Multiscale dynamics of heterogeneous media in the peridynamic formulation. J Elast 106(1):71–103
- Askari E, Bobaru F, Lehoucq R, Parks ML, Silling SA, Weckner O (2008) Peridynamics for multiscale materials modeling. J Phys: Conf Ser 125:012078. IOP Publishing
- You H, Yu Y, Kamensky D (2020) An asymptotically compatible formulation for local-to-nonlocal coupling problems without overlapping regions. Comput Methods Appl Mech Eng 366:113038
- Scalas E, Gorenflo R, Mainardi F (2000) Fractional calculus and continuous time finance. Phys A 284: 376–384
- D'Elia M, Du Q, Gunzburger M, Lehoucq R (2017) Nonlocal convection-diffusion problems on bounded domains and finite-range jump processes. Comput Methods Appl Math 29:71–103
- Meerschaert MM, Sikorskii A (2019) Stochastic models for fractional calculus (vol. 43). Walter de Gruyter GmbH & Co KG.
- Burkovska O, Glusa C, D'Elia M (2020) An optimization-based approach to parameter learning for fractional type nonlocal models. Preprint at http://arxiv.org/abs/2010.03666
- D'Elia M, Gunzburger M (2016) Identification of the diffusion parameter in nonlocal steady diffusion problems. Appl Math Optim 73(2):227–249
- Pang G, D'Elia M, Parks M, Karniadakis GE (2020) nPINNs: nonlocal Physics-Informed Neural Networks for a parametrized nonlocal universal Laplacian operator. Algorithms and Applications. J Comput Phys 422:109760
- Pang G, Lu L, Karniadakis GE (2019) fPINNs: Fractional physics-informed neural networks. SIAM J Sci Comput 41:2603–2626
- Xu X, Foster J (2020) Deriving peridynamic influence functions for one-dimensional elastic materials with periodic microstructure. Preprint at http://arxiv.org/abs/2003.05520



- Xu X, D'Elia M, Foster J (2020) Bond-based peridynamic kernel learning with energy constraint. Preprint at http://arxiv.org/abs/2101.01095
- You H, Yu Y, Trask N, Gulian M, D'Elia M (2021) Data-driven learning of robust nonlocal physics from high-fidelity synthetic data. Comput Methods Appl Mech Eng 374:113553
- Du Q, Tao Y, Tian X (2018) A peridynamic model of fracture mechanics with bond-breaking. J Elast 132(2):197–218
- Fan Y, D'Elia M, Yu Y, Najm HN, Silling S (2023) Bayesian nonlocal operator regression: A data-driven learning framework of nonlocal models with uncertainty quantification. J Eng Mech 149(8):04023049
- Lu F, An Q, Yu Y (2023) Nonparametric learning of kernels in nonlocal operators. J Peridyn Nonlocal Model 1–24
- Silling S (2020) Propagation of a stress pulse in a heterogeneous elastic bar. Sandia Report SAND2020-8197, Sandia National Laboratories
- Weckner O, Silling SA (2011) Determination of nonlocal constitutive equations from phonon dispersion relations. Int J Multiscale Comput Eng 9(6)
- Du Q, Gunzburger M, Lehoucq RB, Zhou K (2013) A nonlocal vector calculus, nonlocal volumeconstrained problems, and nonlocal balance laws. Math Models Methods Appl Sci 23(03):493–540
- 27. Bedford A, Drumheller DS (2023) Introduction to elastic wave propagation. Springer Nature.

Publisher's Note Springer Nature remains neutral with regard to jurisdictional claims in published maps and institutional affiliations.

Springer Nature or its licensor (e.g. a society or other partner) holds exclusive rights to this article under a publishing agreement with the author(s) or other rightsholder(s); author self-archiving of the accepted manuscript version of this article is solely governed by the terms of such publishing agreement and applicable law

Authors and Affiliations

Huaiqian You¹ · Yue Yu¹ · Stewart Silling² · Marta D'Elia³,4

Huaiqian You huy316@lehigh.edu

Stewart Silling sasilli@sandia.gov

Marta D'Elia marta.delia@simulation.science

- Department of Mathematics, Lehigh University, Bethlehem, Pennsylvania, USA
- Center for Computing Research, Sandia National Laboratories, Albuquerque, New Mexico, USA
- 3 Computational Science and Analysis, Sandia National Laboratories, Livermore, California, USA
- Pasteur Labs, Brooklyn, New York, USA

